Heterogeneous Inputs to Central Pattern Generators Can Shape Insect Gaits[*]

Zahra Aminzare[†] and Philip Holmes[‡]

Abstract. In our previous work [*SIAM J. Appl. Dyn. Syst.*, 17 (2018), pp. 626–671], we studied an interconnected bursting neuron model for insect locomotion, and its corresponding phase oscillator model, which at high speed can generate stable tripod gaits with three legs off the ground simultaneously in swing and at low speed can generate stable tetrapod gaits with two legs off the ground simultaneously in swing. However, at low speed several other stable locomotion patterns that are not typically observed as insect gaits may coexist. In the present paper, by adding heterogeneous external input to each oscillator, we modify the bursting neuron model so that its corresponding phase oscillator system produces only one stable gait at each speed, specifically a unique stable tetrapod gait at low speed, a unique stable tripod gait at high speed, and a unique branch of stable transition gaits connecting them. This suggests that control signals originating in the brain and central nervous system can modify gait patterns.

1. Introduction. This paper is based on our previous work [1], in which we studied the effect of stepping frequency on transitions from multiple tetrapod insect gaits with two legs off the ground simultaneously in swing to tripod gaits with three legs off the ground simultaneously in swing. In that paper, we used an ion-channel bursting neuron model to describe each of six mutually inhibitory units that form the central pattern generator (CPG) located in the insect's thorax. Each unit of the CPG contains a system of four ordinary differential equations (ODEs), $\dot{x} = f(x)$, where $x = (v, m, w, s)^\top$ describes transmembrane cell voltages, slow and fast ionic gates, and the dynamics of neurotransmitter release at synapses, respectively. The parameters are chosen such that the model possesses an attracting hyperbolic bursting limit cycle. See Table 2 and Figure 10 (left) in the appendix to this paper. Each unit receives an external current, denoted by I_{ext}, which represents input from the central nervous system and brain. We observe that I_{ext} affects the frequency of the limit cycle and thus acts as a speed parameter (Figure 10 (right)). See [1] or the appendix for more details of the bursting neuron model, its parameter values, and its behavior.

In [1] we assumed that each oscillatory unit drives one leg of the insect and that the units are connected to their nearest neighbors in an homogeneous (identical) network as shown in

---

[†]Department of Mathematics, University of Iowa, Iowa City, IA 52242 (zahra-aminzare@uiowa.edu).

[‡]The Program in Applied and Computational Mathematics, Department of Mechanical and Aerospace Engineering, and Princeton Neuroscience Institute, Princeton University, NJ 08544 (pholmes@math.princeton.edu).
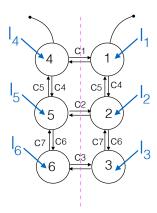
Figure 1. *The network of heterogeneous CPGs with different external inputs, $I_i = I_{ext} + I_{ext}^i(t)$.*

Figure 1, but where input currents are also identical, $I_i = I_{ext}$. Inhibitory coupling between the oscillators is achieved via synapses that produce negative postsynaptic currents. The synapse variable s enters the postsynaptic cell as an additional term: see (23) in the appendix.

Employing phase reduction, we collapsed the network of six homogeneous bursting neurons represented by 24 ODEs to six coupled nonlinear phase oscillators, each corresponding to a sub-network of neurons controlling one leg. Assuming that the left and right legs maintain constant phase differences (contralateral symmetry), we then reduced from six equations to three, allowing analysis of a dynamical system with two phase differences defined on a two-dimensional torus.

With certain balance conditions on the coupling strengths among the homogeneous oscillators, described in section 3 below, we showed that at low speeds, the phase differences model on the torus can generate multiple fixed points, including stable tetrapod and unstable tripod gaits. In contrast, at high speeds, it generates a unique stable tripod gait. Moreover, as speed increases, the gait transition occurs through degenerate bifurcations, at which a subset of the multiple fixed points merge to produce a unique stable fixed point: see [1, Figure 23].

In the current paper, we study this degenerate bifurcation in the phase difference model by unfolding the original system. To this end we relax the condition of homogeneous ion-channel bursting neuron models in the network of CPGs and allow heterogeneous (nonidentical) models by adding different external inputs to each oscillator. We assume that in addition to the external current I_{ext}, each unit receives a different external input denoted by $I_{ext}^i(t)$, where i is the leg number, as shown in Figure 1. We also assume that $I_{ext}^i(t)$ is a time-dependent function with magnitude of order $\mathcal{O}(\bar{g}_{syn})$, where $\bar{g}_{syn}$ is the synaptic strength. We subsequently show that this heterogeneity is equivalent to perturbing the coupling functions or the contralateral coupling strengths in a phase reduced oscillator model, i.e., different types of heterogeneity can have similar effects on dynamics (see section 5 below).

Recent studies of different three-cell ion-channel bursting CPG networks [2, 3, 4] share some common features with the current paper. Without explicitly addressing insect locomotion, or using phase reduction theory, the authors numerically extract Poincaré maps defined on two-dimensional tori which have multiple stable fixed points corresponding to orbits with specific phase differences. In particular, [4] introduces transient control inputs—brief pulses simultaneously applied to all three cells—that can move solutions from one stable state to

another. A more abstract study of coupled cell systems with an emphasis on heteroclinic cycles that lie in "synchronous subspaces" appears in [5].

This paper is organized as follows. In section 2, we review the derivation of phase equations for heterogeneous networks and apply these techniques to the interconnected bursting neuron model. In section 3, we define approximate tetrapod, tripod, and transition gaits for heterogeneous networks and then, by assuming constant phase differences between left- and right-hand oscillators, as in the homogeneous case, we reduce the six phase equations to two phase difference equations. In section 4, we describe the main results of this paper. By choosing appropriate heterogeneous external inputs, we show that the phase differences model possesses only one stable fixed point, which at low speed corresponds to a tetrapod gait and at high speed corresponds to a tripod gait. Interpreting the heterogeneities as small bifurcation parameters, we find cases in which two or three saddle-node bifurcations occur as heterogeneity increases and a unique tetrapod gait emerges from multiple tetrapod gaits and other, ill-defined gaits. This shows that specific fixed points (gaits) can be preserved, or removed, by small external input currents. In section 5, we show that our heterogeneities are equivalent to perturbing the coupling functions or the contralateral coupling strengths in a phase reduced oscillator model. In section 6, we conclude. The appendix reviews the bursting neuron model studied in [1], displaying burst dynamics and the influence of its parameters on speed.

2. A phase oscillator model. To analyze the gait transition mathematically, in [1, section 3], we applied the theory of weakly coupled oscillators to the coupled bursting neuron models to reduce the 24 ODEs to 6 phase oscillator equations. In this section, we derive the phase equations of weakly coupled oscillators with heterogeneous dynamics, i.e., coupled oscillators with different frequencies. We develop the theory in greater generality than our specific applications will demand, allowing time-dependent input currents $I_{ext}^i(t)$.

Let $\dot{x} = f(x)$, $x \in \mathbb{R}^n$, describe the dynamics of a single oscillator and assume that it possesses an attracting hyperbolic limit cycle $\Gamma = \Gamma(t)$, with period T and frequency $\omega = 2\pi/T$. The phase of an oscillator, denoted by ϕ, is the time that has elapsed as its state moves around Γ, starting from an arbitrary reference point in the cycle, called the relative phase.

2.1. Phase equations for weakly coupled heterogeneous oscillators. Consider a pair of weakly coupled heterogeneous oscillators

$$
\begin{aligned}
\dot{x}_1 &= f_1(x_1) + \epsilon g(x_1, x_2), \\
\dot{x}_2 &= f_2(x_2) + \epsilon g(x_2, x_1),
\end{aligned}
\tag{1}
$$

where f_i describes the intrinsic dynamics of each oscillator, $0 < \epsilon \ll 1$ is the coupling strength, and g is the coupling function. For each oscillator, the phase equation can be written as follows. For more details see [1, section 3].

$$
\frac{d\phi_i}{dt}(t) = \omega_i + \epsilon H_i(\phi_j(t) - \phi_i(t)) + \mathcal{O}(\epsilon^2),
\tag{2}
$$

where

$$
H_i = H_i(\theta) = \frac{1}{T_i} \int_0^{T_i} Z_i(\Gamma_i(\tilde{t})) \cdot g(\Gamma_i(\tilde{t}), \Gamma_i(\tilde{t} + \theta)) \, d\tilde{t},
$$

is the coupling function: the convolution of the coupling g and the oscillator's infinitesimal phase response curve (iPRC), Z_i, and ω_i and T_i are respectively the frequency and period of each oscillator described by $\dot{x}_i = f_i(x_i)$. Under the weak coupling assumption, the iPRC captures the local dynamics of each oscillator in a neighborhood of its limit cycle Γ_i; see [6].

Equation (2) is a general phase equation for a pair of weakly coupled heterogeneous oscillators where the heterogeneity is of arbitrary size. This means that the oscillators' frequencies can be very different. But if the frequencies are close to each other, i.e., the heterogeneities are small and in particular are of order of the coupling strength ϵ, then one can approximate (2) as follows [7, Chapter 5].

Assume that $f_i = f + \tilde{f}_i$, where the heterogeneity $\tilde{f}_i$ is of order ϵ, $\mathcal{O}(\epsilon)$. This is equivalent to having identical oscillators with dynamics f, frequency ω, and period T, and nonidentical coupling functions $g_i = g + \tilde{f}_i/\epsilon$. Then (2) can be approximated by the following phase equations:

$$(3) \qquad \frac{d\phi_i}{dt}(t) = \omega + \tilde{\omega}_i + \epsilon H(\phi_j(t) - \phi_i(t)) + \mathcal{O}(\epsilon^2),$$

where

$$H = H(\theta) = \frac{1}{T} \int_0^T Z(\Gamma(\tilde{t})) \cdot g(\Gamma(\tilde{t}), \Gamma(\tilde{t} + \theta)) \, d\tilde{t},$$

is the coupling function, specifically the convolution of the synaptic coupling g with the oscillator's iPRC, Z. Here Z is computed for the limit cycle of $\dot{x} = f(x)$, and the frequency differences are constant shifts of $\mathcal{O}(\epsilon)$:

$$(4) \qquad \tilde{\omega}_i = \frac{1}{T} \int_0^T Z(\Gamma(\tilde{t})) \cdot \tilde{f}_i(\Gamma(\tilde{t})) \, d\tilde{t}.$$

The advantage of this decomposition is that only one iPRC and so only one coupling function must be computed.

Now consider a network of N heterogeneous oscillators with intrinsic dynamics $\dot{x}_i = f_i(x_i)$ and corresponding frequencies ω_i. For $i = 1, \ldots, N$, let

$$(5) \qquad \dot{x}_i = f_i(x_i) + \sum_{j \in \mathcal{N}_i} \epsilon_j g(x_i, x_j)$$

describe the dynamics of each x_i in the weakly coupled network. Here $\mathcal{N}_i$ denotes the neighbors of oscillator i, and ϵ_j denotes the coupling strengths, which are all of $\mathcal{O}(\epsilon)$ for some $0 < \epsilon \ll 1$. As in the case of a pair of coupled oscillators, one can derive phase equations from (5) as follows:

$$(6) \qquad \dot{\phi}_i = \omega + \tilde{\omega}_i + \sum_{j \in \mathcal{N}_i} \epsilon_j H(\phi_j - \phi_i) + \mathcal{O}(\epsilon^2),$$

where the frequency differences $\tilde{\omega}_i$ are as defined in (4).

2.2. Phase equations for six weakly coupled heterogeneous bursting neuron model. We now apply the techniques from section 2.1 to six heterogeneous units in the coupled bursting neuron model and derive the six-coupled phase oscillator model via phase reduction.

In the homogeneous interconnected bursting neuron model, the intrinsic dynamics of each hemisegmental unit, described by $\dot{x} = f(x)$, is identical. We now assume that each hemisegmental unit receives a small heterogeneous external input, i.e., each unit can be described by

$$\dot{x}_i = f_i(x_i) = f(x_i) + I_{ext}^i(t) \cdot \mathbf{e}_1,$$

where $\dot{x}_i = f_i(x_i)$ has an attracting hyperbolic limit cycle with frequency close to the attracting hyperbolic limit cycle of $\dot{x} = f(x)$. For $i = 1, \ldots, 6$, $I_{ext}^i(t)$ is the additional small external input to each unit and represents the weak heterogeneity of the corresponding unit such that $I_{ext}^i(t) = \mathcal{O}(\bar{g}_{syn})$ and $\mathbf{e}_1 = (1, 0, 0, 0)^\top$, i.e., only the voltage equations are heterogeneous.
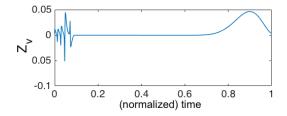
Recalling (6), we can derive approximate phase equations for the coupled bursting neuron model of Figure 1 as follows:

(7)
$$
\begin{aligned}
\dot{\phi}_1 &= \omega + \tilde{\omega}_1 + c_1 H(\phi_4 - \phi_1) + c_5 H(\phi_2 - \phi_1), \\
\dot{\phi}_2 &= \omega + \tilde{\omega}_2 + c_2 H(\phi_5 - \phi_2) + c_4 H(\phi_1 - \phi_2) + c_7 H(\phi_3 - \phi_2), \\
\dot{\phi}_3 &= \omega + \tilde{\omega}_3 + c_3 H(\phi_6 - \phi_3) + c_6 H(\phi_2 - \phi_3), \\
\dot{\phi}_4 &= \omega + \tilde{\omega}_4 + c_1 H(\phi_1 - \phi_4) + c_5 H(\phi_5 - \phi_4), \\
\dot{\phi}_5 &= \omega + \tilde{\omega}_5 + c_2 H(\phi_2 - \phi_5) + c_4 H(\phi_4 - \phi_5) + c_7 H(\phi_6 - \phi_5), \\
\dot{\phi}_6 &= \omega + \tilde{\omega}_6 + c_3 H(\phi_3 - \phi_6) + c_6 H(\phi_5 - \phi_6),
\end{aligned}
$$

where

(8)
$$\tilde{\omega}_i = \frac{1}{T} \int_0^T Z_v(\Gamma(t)) I_{ext}^i(t) dt,$$

and Z_v is the iPRC of the limit cycle of $\dot{x} = f(x)$ in the direction of voltage. In Figure 2 (left), we show Z_v for $I_{ext} = 35.9$, in which the rapid oscillations are due to the burst in the corresponding limit cycle. Note that the averaging theorem and convolution integral used in phase reduction eliminates time dependence in I_{ext}^i. The positive constant c_i's represent the coupling strengths between the oscillators. Following [8], we assume contralateral symmetry and include only nearest neighbor coupling, as shown in Figure 1, so that there are three contralateral coupling strengths c_1, c_2, c_3 and four ipsilateral coupling strengths c_4, c_5, c_6, and c_7.
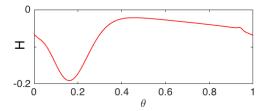

Figure 2. *The iPRC (in the direction of v) (left) and the coupling function $H(\theta)$ (right) for $I_{ext} = 35.9$. Phase $\theta = 0$ is defined to be the onset of the burst. From* [1, *Figure 8*].

Also, the coupling function H takes the following form:

$$(9) \qquad H(\theta) = -\frac{\bar{g}_{syn}}{T} \int_0^T Z_v(\Gamma(t)) \left(v_i(\Gamma(t)) - E_s^{post}\right) s_j \left(\Gamma(t + \theta)\right) \, dt,$$

where E_s^{post}, the reversal potential, is a constant. In Figure 2 (right), we show the coupling function H derived in (9) for $I_{ext} = 35.9$. Note that for $I_{ext} = 35.9$, $H(\theta) < 0$, and for an arbitrary I_{ext}, $H(\theta) < 0$ over most of its range, and in particular over the interval $[1/3, 2/3]$, which we will show contains the tetrapod, tripod, and transition gaits.

To simplify notation, for the remainder of the paper, $T = 1$ and all the phases and the coupling functions are considered in the domain $[0, 1]$ instead of $[0, 2\pi]$.

Figure 2 shows a typical iPRC and the corresponding coupling function for bursting neurons with inhibitory synapses like those used throughout the current paper and in [1]. Other forms are also found (e.g., see [9, Figure 8]), and sinusoidal coupling functions were fitted to experimental cockroach data in [8, Figure 2]. However, in [1, section 6, Proposition 11] we prove that a general class of functions exists that satisfy Assumption 1 and (10) below, and which therefore produce tetrapod to tripod gait transitions. We henceforth assume that our coupling functions $H(\theta; \xi)$ satisfy these conditions.

3. Reduced phase equations. In this section, the goal is to reduce the six equations (7) to two equations on a 2-torus. Although we are interested in gaits generated by the bursting neuron model and its phase reduction equations (7), we prove our results for a more general case. To this end, we assume that the following conditions hold for the coupling function H and the external inputs $I_{ext}^i(t)$. We let H and the frequency ω depend on the speed parameter ξ and write $H = H(\theta; \xi)$ and $\omega = \omega(\xi)$.

Assumption 1. Let $H = H(\theta; \xi)$ be a differentiable function, defined on $\mathbb{R} \times [\xi_1, \xi_2]$ which is 1-periodic on its first argument and has the following property. For any fixed $\xi \in [\xi_1, \xi_2]$,

$$(10) \qquad H\left(\frac{2}{3} - \eta; \xi\right) = H\left(\frac{1}{3} + \eta; \xi\right)$$

has a unique solution $\eta(\xi)$ such that $\eta = \eta(\xi) : [\xi_1, \xi_2] \to [0, 1/6]$ is an onto and nondecreasing function. Note that (10) is also trivially satisfied by the constant solution $\eta = 1/6$.

Assumption 1 defines a class of coupling functions that exhibit the gait transitions studied here and in [1]. The coupling functions derived from the bursting neuron model satisfy and motivate this assumption; see [1, Figure 9]. For the rest of the paper, we assume that the coupling function H satisfies Assumption 1.

Assumption 2. For $i = 1, 2, 3$, let $I_{ext}^{i+3}(t) = I_{ext}^i(t)$. This assumption maintains contralateral symmetry. In addition, we assume that for $i = 1, 2, 3$, $I_{ext}^i(t)$ are not equal; otherwise the system becomes homogeneous.

Assumption 3. Let the coupling strengths satisfy the following balance condition:

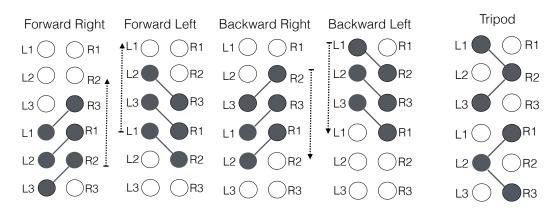$$(11) \qquad c_1 + c_5 = c_2 + c_4 + c_7 = c_3 + c_6.$$

Figure 3. *Left to right: One cycle of forward right, forward left, backward right, and backward left tetrapod gaits and a tripod gait are shown. The diagonal lines connect legs that swing together; arrows indicate forward (resp., backward) waves in tetrapods. The tripod is a standing wave. Adapted from* [1, *Figure 4*].

Equation (11) expresses the fact that the sum of the coupling strengths entering each leg are equal. The equalities were assumed, without biological support, in [9] and were subsequently found to approximately hold for fast running cockroaches in [8, Figure 9c], according to the best data fits, judged by Akaike and Bayes information criteria, as also noted in [1, section 1]. In [1, Proposition 3 and Corollary 4] we proved that when the coupling strengths satisfy the balance condition, in the homogeneous case $\tilde{\omega}_i = 0$, (7) admits tetrapod gaits at low speeds and tripod gaits at high speeds.

In what follows we define "approximate gaits." These definitions are consistent with Assumptions 1–3 in the presence of heterogeneity in our model.

3.1. Gait definitions: Generalization to heterogeneous systems. In [1, Definition 1] we defined four versions of tetrapod gaits and a tripod gait. Figure 3 shows cartoons of an insect executing one cycle of the tetrapod and tripod gaits, in which each leg completes one swing and one stance phase. Each gait corresponds to a 1-periodic solution of (7) with $\tilde{\omega}_i = 0$. In what follows, we generalize those definitions to heterogeneous models, i.e., (7) with at least one $\tilde{\omega}_i \neq 0$.

Definition 1 (approximate tetrapod and tripod gaits). *The approximate gaits, denoted by* A_T^p, *are 1-periodic solutions of* (7) *with at least one* $\tilde{\omega}_i \neq 0$:

$$A_T^p := (\hat{\omega}t + \psi_1 + \delta_1,\ \hat{\omega}t + \psi_2 + \delta_2,\ \hat{\omega}t + \psi_3 + \delta_3;\ \hat{\omega}t + \psi_1 + \delta_1 + \psi,$$
$$\hat{\omega}t + \psi_2 + \delta_2 + \psi,\ \hat{\omega}t + \psi_3 + \delta_3 + \psi)^\top,$$

where $\hat{\omega}$ *is a coupled stepping frequency that all six oscillators share,*

$$(12) \quad \begin{aligned} \hat{\omega} &= \omega(\xi) + c_1 H(\psi; \xi) + c_5 H(\psi_2 - \psi_1; \xi) \\ &= \omega(\xi) + c_2 H(\psi; \xi) + c_4 H(\psi_1 - \psi_2; \xi) + c_7 H(\psi_3 - \psi_2; \xi) \\ &= \omega(\xi) + c_3 H(\psi; \xi) + c_6 H(\psi_2 - \psi_3; \xi), \end{aligned}$$

ψ_1, ψ_2, ψ_3 *are corresponding relative phases, and* ψ *is the corresponding constant contralateral phase difference in approximate gaits. Note that the equalities in* $\hat{\omega}$ *hold by Assumptions* 1 *and* 3.

The δ_i's are perturbations to the legs' phases due to the heterogeneity and are the solutions of

$$\begin{pmatrix} \tilde{\omega}_1 \\ \tilde{\omega}_2 \\ \tilde{\omega}_3 \end{pmatrix} = \mathcal{L}(\psi_1, \psi_2, \psi_3) \begin{pmatrix} \delta_1 \\ \delta_2 \\ \delta_3 \end{pmatrix},$$

where

$$\mathcal{L}(\psi_1, \psi_2, \psi_3)$$
$$= \begin{pmatrix} c_5 H'(\psi_2 - \psi_1; \xi) & -c_5 H'(\psi_2 - \psi_1; \xi) & 0 \\ -c_4 H'(\psi_1 - \psi_2; \xi) & c_4 H'(\psi_1 - \psi_2; \xi) + c_7 H'(\psi_3 - \psi_2; \xi) & -c_7 H'(\psi_3 - \psi_2; \xi) \\ 0 & -c_6 H'(\psi_2 - \psi_3; \xi) & c_6 H'(\psi_2 - \psi_3; \xi) \end{pmatrix},$$

and H' denotes the derivative of H w.r.t. its first argument. The matrix $\mathcal{L}$ is singular, so we let $(\delta_1, \delta_2, \delta_3)^\top = \mathcal{L}^+(\tilde{\omega}_1, \tilde{\omega}_2, \tilde{\omega}_3)^\top$, where $\mathcal{L}^+$ is the generalized inverse (pseudoinverse) of $\mathcal{L}$; see [10].

The following choices of the relative phases ψ_1, ψ_2, ψ_3 and the contralateral phase difference ψ give four different versions of approximate tetrapod gaits and an approximate tripod gait:

1. *The approximate forward right tetrapod gait, denoted by A_{FR}^p, corresponds to A_T^p with $\psi_1 = 2/3, \psi_2 = 0, \psi_3 = 1/3$, and $\psi = 2/3$.*
2. *The approximate forward left tetrapod gait, denoted by A_{FL}^p, corresponds to A_T^p with $\psi_1 = 2/3, \psi_2 = 0, \psi_3 = 1/3$, and $\psi = 1/3$.*
3. *The approximate backward right tetrapod gait, denoted by A_{BR}^p, corresponds to A_T^p with $\psi_1 = 1/3, \psi_2 = 0, \psi_3 = 2/3$, and $\psi = 1/3$.*
4. *The approximate backward left tetrapod gait, denoted by A_{BL}^p, corresponds to A_T^p with $\psi_1 = 1/3, \psi_2 = 0, \psi_3 = 2/3$, and $\psi = 2/3$.*
5. *The approximate tripod gait, denoted by A_{Tri}^p, corresponds to A_T^p with $\psi_1 = 1/2, \psi_2 = 0, \psi_3 = 1/2$, and $\psi = 1/2$.*

In forward tetrapod gaits a wave of swing phases runs from hind to front legs and in backward tetrapod gaits the swing phases run from front to hind legs, as shown by arrows in Figure 3.

The matrix $\mathcal{L}$ in Definition 1 can be derived by substituting A_T^p into (7) and approximating H by the first two terms of its Taylor expansion. For instance, substituting A_T^p into the first equation of (7), we get

$$\hat{\omega} = \dot{\phi}_1 = \omega + \tilde{\omega}_1 + c_1 H(\psi; \xi) + c_5 H(\psi_2 + \delta_2 - \psi_1 - \delta_1; \xi)$$
$$= \omega + \tilde{\omega}_1 + c_1 H(\psi; \xi) + c_5 H(\psi_2 - \psi_1; \xi) + c_5 H'(\psi_2 - \psi_1; \xi)(\delta_2 - \delta_1) + \mathcal{O}(\delta_2 - \delta_1)^2.$$

By substituting $\hat{\omega} = \omega(\xi) + c_1 H(\psi; \xi) + c_5 H(\psi_2 - \psi_1; \xi)$ into the above equation, $\tilde{\omega}_1$ can be approximated by $-c_5 H'(\psi_2 - \psi_1; \xi)(\delta_2 - \delta_1)$, which gives the first row of $\mathcal{L}$. The other rows are found in the same way.

Note that when $\delta_i = 0$, i.e., in the homogeneous system, two (resp., three) legs swing simultaneously in tetrapod (resp., tripod) gaits, but when $\delta_i \neq 0$, the corresponding legs do not swing exactly together due to the small perturbations δ_i, so we call them *approximate tetrapod* (resp., *tripod*) *gaits*.

In [1] we showed that (7) admits a solution at a tetrapod gait when the speed parameter ξ is small and a solution at a tripod gait when ξ is large. To connect tetrapod gaits to tripod gaits, we defined transition gaits [1, Definition 2]. In what follows we generalize those definitions for heterogeneous models to connect approximate tetrapod gaits to approximate tripod gaits.

Definition 2 (approximate transition gaits). *For any fixed number $\eta \in [0, 1/6]$,*
1. *the approximate forward right transition gait, denoted by $A_{FR}^p(\eta)$, corresponds to A_T^p with $\psi_1 = 2/3 - \eta, \psi_2 = 0, \psi_3 = 1/3 + \eta$, and $\psi = 2/3 - \eta$;*
2. *the approximate forward left transition gait, denoted by $A_{FL}^p(\eta)$, corresponds to A_T^p with $\psi_1 = 2/3 - \eta, \psi_2 = 0, \psi_3 = 1/3 + \eta$, and $\psi = 1/3 + \eta$;*
3. *the approximate backward right transition gait, denoted by $A_{BR}^p(\eta)$, corresponds to A_T^p with $\psi_1 = 1/3 + \eta, \psi_2 = 0, \psi_3 = 2/3 - \eta$, and $\psi = 1/3 + \eta$;*
4. *the approximate backward left transition gait, denoted by $A_{BL}^p(\eta)$, corresponds to A_T^p with $\psi_1 = 1/3 + \eta, \psi_2 = 0, \psi_3 = 2/3 - \eta$, and $\psi = 2/3 - \eta$.*

As ξ increases, $\eta = \eta(\xi)$, the solution of (10), varies from 0 to 1/6. Therefore, at low speeds, when $\eta = 0$, $A_{FR}^p(\eta)$ (resp., $A_{FL}^p(\eta)$, $A_{BR}^p(\eta)$, and $A_{BL}^p(\eta)$) corresponds to the approximate forward right (resp., forward left, backward right, and backward left) transition gait, and as ξ increases and η approaches 1/6, all the approximate transition gaits tend to an approximate tripod gait.

In what follows, we will see how certain properties of H allow us to reduce six phase equations to three ipsilateral equations.

In both approximate tetrapod and tripod gaits, the phase difference between the left and right legs, denoted by ψ, is constant and is equal to either $\psi = 1/3$ or $\psi = 2/3$ (in tetrapod gaits) or $\psi = 1/2$ (in the tripod gait). In addition, we observe that the phase differences between the left and right legs in approximate transition gaits are constant and equal to $2/3 - \eta$ or $1/3 + \eta$. For steady states, this assumption is supported by experiments for tripod gaits [8] and by simulations for tripod and tetrapod gaits in the bursting neuron model [1, Figures 4 and 5].

We make a further simplifying assumption that the steady state contralateral phase differences remain constant for all t.

Assumption 4. The phase differences between the left and right legs are constant. For $i = 1, 2, 3$,
$$\phi_{i+3} - \phi_i = 2/3 - \eta \quad \text{or} \quad \phi_{i+3} - \phi_i = 1/3 + \eta.$$

As discussed earlier, the coupling function computed from the bursting neuron model satisfies Assumption 1 and (10) and thus allows reduction to three ipsilateral equations, as we now describe.

3.2. Phase differences model. In this section, the goal is to reduce the six equations (7) to two equations on a 2-torus.

By Assumptions 1, 2, and 4, (7) can be reduced to the following three equations describing the right legs' motions:

$$(13a) \qquad \dot{\phi}_1 = \omega(\xi) + \tilde{\omega}_1 + c_1 H\left(\frac{2}{3} - \eta; \xi\right) + c_5 H(\phi_2 - \phi_1; \xi),$$

$$(13b) \qquad \dot{\phi}_2 = \omega(\xi) + \tilde{\omega}_2 + c_2 H\left(\frac{2}{3} - \eta; \xi\right) + c_4 H(\phi_1 - \phi_2; \xi) + c_7 H(\phi_3 - \phi_2; \xi),$$

$$(13c) \qquad \dot{\phi}_3 = \omega(\xi) + \tilde{\omega}_3 + c_3 H\left(\frac{2}{3} - \eta; \xi\right) + c_6 H(\phi_2 - \phi_3; \xi).$$

Because only phase differences appear in the vector field, we may define

$$\theta_1 := \phi_1 - \phi_2 \quad \text{and} \quad \theta_2 := \phi_3 - \phi_2,$$

so that, from (13), the following equations describe the dynamics of θ_1 and θ_2:

$$(14a) \qquad \dot{\theta}_1 = \tilde{\omega}_1 - \tilde{\omega}_2 + (c_1 - c_2) H\left(\frac{2}{3} - \eta; \xi\right) + c_5 H(-\theta_1; \xi) - c_4 H(\theta_1; \xi) - c_7 H(\theta_2; \xi),$$

$$(14b) \qquad \dot{\theta}_2 = \tilde{\omega}_3 - \tilde{\omega}_2 + (c_3 - c_2) H\left(\frac{2}{3} - \eta; \xi\right) + c_6 H(-\theta_2; \xi) - c_4 H(\theta_1; \xi) - c_7 H(\theta_2; \xi),$$

where the $\tilde{\omega}_i$'s and H are defined in (8) and (9), respectively. Note that (14) are 1-periodic in both variables, i.e., $(\theta_1, \theta_2) \in \mathbb{T}^2$, where $\mathbb{T}^2$ is a 2-torus. The flows that they generate should not be confused with the Poincaré maps on $\mathbb{T}^2$ derived in [2, 3, 4].

In (14), the approximate tripod gait A^p_{Tri} corresponds approximately to the fixed point $(1/2, 1/2)$, the approximate forward tetrapod gaits, A^p_{FR} and A^p_{FL}, correspond approximately to the fixed point $(2/3, 1/3)$, the approximate backward tetrapod gaits, A^p_{BR} and A^p_{BL}, correspond approximately to the fixed point $(1/3, 2/3)$, and the approximate transition gaits, $A^p_{FR}(\eta)$ and $A^p_{FL}(\eta)$ (resp., $A^p_{BR}(\eta)$ and $A^p_{BL}(\eta)$), correspond approximately to $(2/3 - \eta, 1/3 + \eta)$ (resp., $(1/3 + \eta, 2/3 - \eta)$). See [11] for similar definitions of tetrapod and tripod gaits on a torus.

In [1] we observed that when ξ is small, the forward tetrapod gaits are not the only solutions and there exist some other stable and unstable solutions (e.g., stable or unstable backward tetrapod and unstable tripod gaits). We showed that as ξ increases, one stable tripod gait emerges, through a degenerate bifurcation. In the present work, we show how heterogeneity, $I^i_{ext}(t)$, can break the degenerate bifurcation into separate saddle-node bifurcations such that at low speed, only one stable (either forward or backward tetrapod) gait exists. We are primarily interested in the existence of approximate *forward* tetrapod gaits, since they have been observed widely in insects (section 4.1 below). However, backward tetrapod gaits have also been seen in backward-walking fruit flies [12, Supplementary Materials, Figure S1], and so in section 4.2 we show that $I^i_{ext}(t)$ can be chosen such that an approximate stable backward tetrapod gait exists at low speed.

4. Main results. In this section, we fix a low speed parameter (e.g., $I_{ext} = 35.65$) for which the homogeneous bursting neuron model (23) generates tetrapod gaits. We assume that the balance condition holds, so several fixed points including the forward $(2/3, 1/3)$ and backward $(1/3, 2/3)$ tetrapod gaits exist. The main goal is to show how adding small heterogeneous external currents $I^i_{ext}(t)$ can successively remove fixed points on the torus while respectively preserving the stable forward (see section 4.1 below) or stable backward (see section 4.2 below) tetrapod gaits.

For example, consider the following randomly generated coupling strengths c_i that satisfy the balance condition:

(15)
$$c_1 = 0.8147,\ c_2 = 0.9058,\ c_3 = 0.1270,\ c_4 = 0.9134,\ c_5 = 1.6368,\ c_6 = 2.3245,\ c_7 = 0.6323.$$

Let $I_{ext}^1(t) = I_{ext}^2(t) = \delta I$, where δI is a nonnegative constant, and let $I_{ext}^3(t) = 0$. Note that for $\delta I = 0$, the system becomes homogeneous. Therefore, we consider δI as a heterogeneity parameter and vary it from 0. Figure 4 (left to right) shows the nullclines of (14) with $\delta I \approx 0, 0.02, 0.032, 0.038$, respectively. In this example, for the homogeneous model with $\delta I = 0$, there exist three stable sinks, two unstable sources, and five saddle points. As the heterogeneity parameter δI increases to $\delta I \approx 0.02$, the isolated $\dot{\theta}_2 = 0$ nullcline loop combines with the $\dot{\theta}_2 = 0$ nullcline that encircles the torus and thereafter the number of fixed points reduces to 8 from 10, through a saddle-node bifurcation. As δI increases further, two saddle-node bifurcations occur at approximately $\delta I \approx 0.032, 0.038$ and one stable fixed point located at $\approx (0.71, 0.25)$ remains, which corresponds to a stable approximate forward tetrapod gait. The other three remaining fixed points are a source and two saddle points.

Note that the balance condition is sufficient for the existence of forward and backward tetrapod gaits but does not guarantee their stability. Assuming that the balance condition holds, in [1, Proposition 6](resp., [1, Proposition 7]) we proved that the forward (resp., backward) tetrapod gait is always stable if $c_1 = c_2 = c_3$, and $\alpha := \frac{c_4}{c_4 + c_7} < \alpha_{max}$ (resp., $\alpha > \alpha_{min}$), where α_{max} (resp., α_{min}) can be computed from the derivatives of H:

(16)
$$\alpha_{max}(\xi) := \frac{H'\left(\frac{1}{3}; \xi\right)}{H'\left(\frac{1}{3}; \xi\right) - H'\left(\frac{2}{3}; \xi\right)}, \quad \alpha_{min}(\xi) := \frac{H'\left(\frac{2}{3}; \xi\right)}{H'\left(\frac{2}{3}; \xi\right) - H'\left(\frac{1}{3}; \xi\right)}.$$
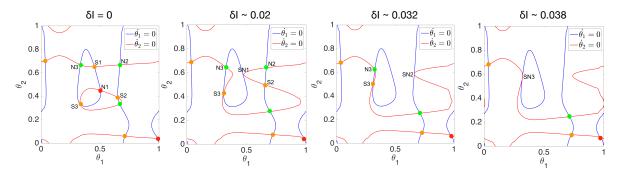

Figure 4. *(Left to right) Nullclines of* (14) *when c_i's satisfy* (15), *$I_{ext} = 35.65$, and $\delta I \approx 0, 0.02, 0.032, 0.038$, respectively. $\dot{\theta}_1 = 0$ nullcline shown in blue; $\dot{\theta}_2 = 0$ nullcline shown in red. Green dots indicate sinks, red dots are sources, and orange dots are saddle points. At $\delta I \approx 0.02$, the first saddle-node bifurcation (shown by SN1) occurs and the unstable tripod gait (shown by N1) disappears together with a saddle point (shown by S1). At $\delta I \approx 0.032$, the second saddle-node bifurcation (shown by SN2) occurs and a stable fixed point (shown by N2) disappears together with a saddle point (shown by S2). Finally, at $\delta I \approx 0.038$, the third saddle-node bifurcation (shown by SN3) occurs and the stable backward tetrapod gait (shown by N3) disappears together with a saddle point (shown by S3). A single stable approximate forward tetrapod gait remains together with a source and two saddle points.*

We further showed that through a transcritical bifurcation at $\alpha = \alpha_{max}$ (resp., $\alpha = \alpha_{min}$), the stable forward (resp., backward) tetrapod gait loses its stability and becomes a saddle point [1, section 5].

For the fixed speed parameter $\xi = I_{ext} = 35.65$, $\alpha_{max} \approx 0.86$ and $\alpha_{min} \approx 0.14$.

Without loss of generality, we can assume that one of the coupling strengths is equal to 1. For the rest of the paper we assume that $c_4 = 1$, the balance condition (11) holds, and $c_1 = c_2 = c_3$. Therefore, by making a change of time variable that eliminates $c_5 = c_6 = 1 + c_7 = 1/\alpha$, (14) can be written as

$$\dot{\theta}_1 = \alpha(\tilde{\omega}_1 - \tilde{\omega}_2) + H(-\theta_1; \xi) - \alpha H(\theta_1; \xi) - (1 - \alpha) H(\theta_2; \xi), \tag{17a}$$

$$\dot{\theta}_2 = \alpha(\tilde{\omega}_3 - \tilde{\omega}_2) + H(-\theta_2; \xi) - \alpha H(\theta_1; \xi) - (1 - \alpha) H(\theta_2; \xi), \tag{17b}$$

which possess both forward and backward tetrapod gaits with stabilities dependent on the value of α.

In section 4.1, we assume $\alpha < \alpha_{max}$ and let $I_{ext}^1(t) = I_{ext}^2(t) = \delta I_f$, where $\delta I_f \geq 0$ is a constant, and $I_{ext}^3(t) = 0$. We show that for some small value of the heterogeneity parameter δI_f, (17) possess only one stable forward tetrapod gait (together with a source and two saddle points).

In section 4.2, we assume $\alpha > \alpha_{min}$ and let $I_{ext}^2(t) = I_{ext}^3(t) = \delta I_b$, where $\delta I_b \geq 0$ is a constant, and $I_{ext}^1(t) = 0$. We show that for some small value of the heterogeneity parameter δI_b, (17) possess only one stable backward tetrapod gait (together with a source and two saddle points).

4.1. Emergence of a unique stable forward tetrapod gait at low speed.
We assume $\alpha < \alpha_{max}$ so that the forward tetrapod gait, $(2/3, 1/3)$, is stable while the backward tetrapod gait can be either stable or a saddle, as described above. For any t, let

$$I_{ext}^1(t) = I_{ext}^2(t) = \delta I_f \geq 0, \quad I_{ext}^3(t) = 0, \tag{18}$$

where δI_f is a nonnegative constant and represents the heterogeneity. We regard δI_f as a bifurcation parameter.

Choosing $I_{ext}^i(t)$ as in (18) implies $\tilde{\omega}_1 - \tilde{\omega}_2 = 0$, and $\tilde{\omega}_3 - \tilde{\omega}_2 = -\delta I_f \bar{Z} \leq 0$, where $\bar{Z} = \frac{1}{T} \int_0^T Z_v(\Gamma(t)) \, dt > 0$ is the average of the phase response curve. Therefore, (17) become

$$\dot{\theta}_1 = H(-\theta_1; \xi) - \alpha H(\theta_1; \xi) - (1 - \alpha) H(\theta_2; \xi), \tag{19a}$$

$$\dot{\theta}_2 = -\alpha \delta I_f \bar{Z} + H(-\theta_2; \xi) - \alpha H(\theta_1; \xi) - (1 - \alpha) H(\theta_2; \xi). \tag{19b}$$

Equations (19) can also be obtained if $I_{ext}^1(t) = I_{ext}^2(t) = 0$, $I_{ext}^3(t) = \delta I_f < 0$.

Figure 5 shows that as α decreases and approaches α_{min}, one of the saddle points moves toward the position of the backward tetrapod gait, which is shown by an arrow in Figure 5 (left), and through a transcritical bifurcation at $\alpha = \alpha_{min}$, the backward tetrapod gait (shown by N) becomes a saddle point and the saddle point becomes a stable node, as expected [1, Proposition 7]. As α decreases further, through a saddle-node bifurcation the stable node and another saddle (shown by S) disappear. We call the bifurcation point $\bar{\alpha}_{min}$, which is smaller
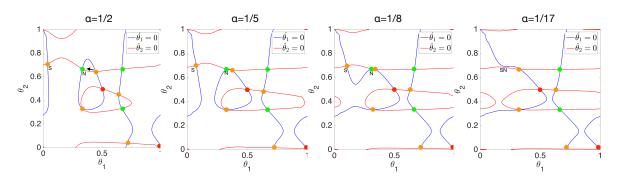
Figure 5. *(Left to right) Nullclines of* (19) *with* $\alpha = 1/2, 1/5, 1/8, 1/17$, $I_{ext} = 35.65$, *and* $\delta I_f = 0$, *respectively. At* $\alpha = 1/2$, *there exist* 10 *fixed points including one stable backward tetrapod gait shown by N. As* α *decreases and reaches* α_{min}, *a saddle point moves (shown by an arrow) toward the backward tetrapod gait N, which loses its stability in a transcritical bifurcation, becoming a saddle point. The stable node N continues to move leftward and as* α *reaches* $\bar{\alpha}_{min}$, *N and the left most saddle point S disappear in a saddle-node bifurcation SN. The stable forward tetrapod and a stable fixed point at* $\approx (2/3, 2/3)$ *remain throughout. Nullclines and fixed points are colored as indicated in Figure* 4.

than α_{min}. Note that as α decreases and reaches $\bar{\alpha}_{min}$, the isolated $\dot{\theta}_1 = 0$ nullcline loop combines with the $\dot{\theta}_1 = 0$ nullcline that encircles the torus and thereafter the number of fixed points decreases from 10 to eight. Thus, for $0 < \alpha < \bar{\alpha}_{min}$, there are only eight fixed points.

Therefore, we consider two topologically different cases:

$\bar{\alpha}_{min} < \alpha < \alpha_{max}$. At $\delta I_f = 0$, (19) admits ten fixed points (five saddle points, three sinks, and two sources). As δI_f increases, three saddle-node bifurcations occur and one sink (corresponding to the approximate forward tetrapod gait), one source, and two saddle points remain. Note that at $\alpha = \alpha_{min}$, a transcritical bifurcation occurs. However, the number of fixed points or the number of stability types does not change.

$0 < \alpha < \bar{\alpha}_{min}$. At $\delta I_f = 0$, (19) admits eight fixed points (four saddle points, two sinks, and two sources). As δI_f increases, two saddle-node bifurcations occur and one sink (corresponding to the approximate forward tetrapod gait), one source, and two saddle points remain.

Three saddle-node bifurcations: $\bar{\alpha}_{min} < \alpha < \alpha_{max}$. Consider (19) with $\bar{\alpha}_{min} < \alpha < \alpha_{max}$. Since the qualitative behavior of the solutions of (19) with $\bar{\alpha}_{min} < \alpha < \alpha_{max}$ are all similar, we show the results in an example with $\alpha = 1/2$. As is clear from (19) and illustrated in Figure 6 (first row), choosing the heterogeneity of (18) maintains the $\dot{\theta}_1 = 0$ nullclines and only perturbs the $\dot{\theta}_2 = 0$ nullclines. This perturbation causes the topology of the $\dot{\theta}_2 = 0$ nullclines to change, combining the isolated closed curve of the $\dot{\theta}_2 = 0$ nullcline with a nullcline that encircles the torus and thereafter reduces the number of fixed points. In this case, where $\alpha = 1/2$, at $\delta I_f = 0$, there exist three stable sinks, two unstable sources, and five saddle points. As δI_f increases and reaches $\delta I_f \approx 0.011$, a saddle-node bifurcation (shown by SN1) occurs and the unstable tripod gait (shown by N1) disappears together with a saddle point (shown by S1); as δI_f increases further to 0.025 another saddle-node bifurcation (shown by SN2) occurs and a stable fixed point (shown by N2) disappears together with a saddle point (shown by S2). Finally, at $\delta I_f \approx 0.037$, the third saddle-node bifurcation (shown by
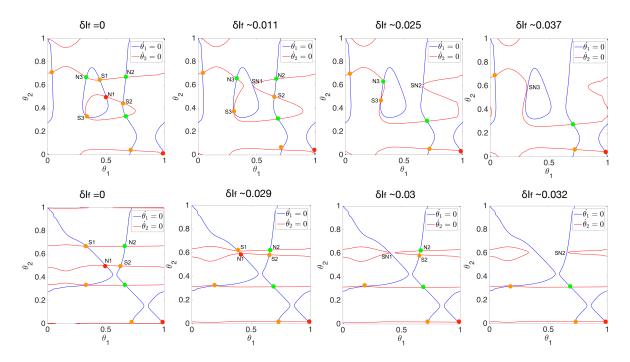
Figure 6. *Nullclines of* (17) *with* $I_{ext} = 35.65$ *are shown for* $\alpha = 1/2$ *(first row) and* $\alpha \approx 0.03$ *(second row) as the heterogeneity parameter* δI_f *varies. As discussed in section* 4.1, (17) *with* $\delta I_f = 0$ *possess either* 10 *(first row, left) or eight (second row, left) fixed points including a stable forward tetrapod gait. As* δI_f *increases, through three (first row) or two (second row) saddle-node bifurcations (shown by SN), six (first row) or four (second row) fixed points disappear and a single stable approximate forward tetrapod gait remains together with a source and two saddle points. Note that in the second row the second to left figure is topologically equivalent to the left figure and is included to show how the nullclines move. Nullclines and fixed points are colored as indicated in Figure* 4.

SN3) occurs and the stable backward tetrapod gait (shown by N3) disappears together with a saddle point (shown by S3). A single stable approximate forward tetrapod gait remains together with a source and two saddle points.

Two saddle-node bifurcations: $0 < \alpha < \bar{\alpha}_{min}$. We now consider (19) with $\alpha < \bar{\alpha}_{min}$. Since the qualitative behavior of the solutions of (19) with $0 < \alpha < \bar{\alpha}_{min}$ are all similar, we only show the results for $\alpha \approx 0.03$. As illustrated in Figure 6 (second row), choosing the heterogeneity of (18) maintains the $\dot{\theta}_1 = 0$ nullclines and, by combining two nullclines that encircle the torus, changes the topology of the $\dot{\theta}_2 = 0$ nullclines and thereafter, through two saddle-node bifurcations, reduces the number of fixed points. As δI_f increases from 0 to 0.03, one saddle-node bifurcation occurs (shown by SN1) in which the unstable tripod gait (shown by N1) and the backward tetrapod gait (shown by S1) disappear; as δI_f increases further to 0.032, another saddle-node bifurcation occurs (shown by SN2) and the stable fixed point on $\theta_1 = \theta_2$ (shown by N2) disappears and a unique stable approximate forward tetrapod gait remains at $(0.69, 0.31)$. The nullclines at $\delta I_f \approx 0.029$ are shown to illustrate how the nullclines move toward each other and cause the saddle-node bifurcations.

So far, we assumed that the forward tetrapod gait is always stable and chose the control parameters $I_{ext}^i(t)$ to get a unique stable approximate forward tetrapod gait. In the following section, we assume that the backward tetrapod gait is always stable and show how to choose $I_{ext}^i(t)$ to get a unique stable approximate backward tetrapod gait. As discussed earlier, when $\alpha_{min} < \alpha$, the backward tetrapod gait is always stable.

4.2. Emergence of a unique backward tetrapod gait at low speed. We assume $\alpha_{min} < \alpha$ so that the backward tetrapod gait, $(1/3, 2/3)$, is stable while the forward tetrapod gait can be either stable or a saddle.

For any t, let

$$(20) \qquad I_{ext}^2(t) = I_{ext}^3(t) = \delta I_b \ \geq \ 0, \quad I_{ext}^1(t) = 0,$$

where δI_b is a nonnegative constant and represents the heterogeneity. We consider δI_b as a bifurcation parameter.

Choosing $I_{ext}^i(t)$ as in (20) implies $\tilde{\omega}_3 - \tilde{\omega}_2 = 0$, and $\tilde{\omega}_1 - \tilde{\omega}_2 = -\delta I_b \bar{Z} \leq 0$. Therefore, (17) become

$$(21a) \qquad \dot{\theta}_1 = -\alpha \delta I_b \bar{Z} + H(-\theta_1; \xi) - \alpha H(\theta_1; \xi) - (1 - \alpha)H(\theta_2; \xi),$$

$$(21b) \qquad \dot{\theta}_2 = H(-\theta_2; \xi) - \alpha H(\theta_1; \xi) - (1 - \alpha)H(\theta_2; \xi).$$

Figure 7 shows that as α increases and approaches α_{max}, one of the saddle points moves toward the position of the forward tetrapod gait, which is shown by an arrow in Figure 7 (left), and through a transcritical bifurcation at $\alpha = \alpha_{max}$, the forward tetrapod gait (shown by N) becomes a saddle point and the saddle point becomes a stable node, as expected [1, Proposition 6]. As α increases further, through a saddle-node bifurcation, the stable node and another saddle point (shown by S) disappear. We call the bifurcation point $\bar{\alpha}_{max}$ which is
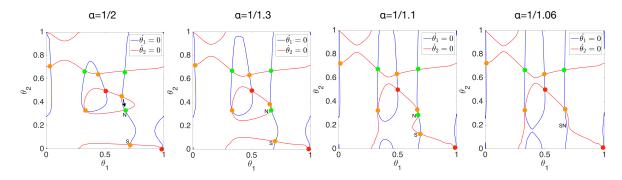

Figure 7. *(Left to right) Nullclines of* (21) *with* $\alpha = 1/2, 1/1.3, 1/1.1, 1/1.06$, $I_{ext} = 35.65$, *and* $\delta I_b = 0$, *respectively. At* $\alpha = 1/2$, *there exist* 10 *fixed points including one stable forward tetrapod gait shown by N. As* α *increases and reaches* α_{max}, *a saddle point moves (shown by an arrow) toward N, which loses its stability in a transcritical bifurcation, becoming a saddle point. The stable node N continues to move downward and, as* α *reaches* $\bar{\alpha}_{max}$, N *and the lowest saddle point* S *disappear in a saddle-node bifurcation* SN. *The stable backward tetrapod and a stable fixed point at* $\approx (2/3, 2/3)$ *remain throughout. Nullclines and fixed points are colored as indicated in Figure* 4.

bigger than α_{max}. Note that as α increases, the isolated $\dot{\theta}_2 = 0$ nullcline loop combines with the $\dot{\theta}_2 = 0$ nullcline that encircles the torus and thereafter, at $\alpha = \bar{\alpha}_{max}$, the number of fixed points reduces to eight from 10. Thus, when $\alpha > \bar{\alpha}_{max}$, there are only eight fixed points.

Therefore, we consider two topologically different cases:

$\alpha_{min} < \alpha < \bar{\alpha}_{max}$. At $\delta I_b = 0$, (21) admits ten fixed points (five saddle points, three sinks, and two sources). As δI_b increases, three saddle-node bifurcations occur and one sink (corresponding to the approximate backward tetrapod gait), one source, and two saddle points remain. Note that at $\alpha = \alpha_{max}$, a transcritical bifurcation occurs. However, the number of fixed points or the number of stability types does not change.

$\alpha > \bar{\alpha}_{max}$. At $\delta I_b = 0$, (21) admits eight fixed points (four saddle points, two sinks, and two sources). As δI_b increases, two saddle-node bifurcations occur and one sink (corresponding to the approximate backward tetrapod gait), one source, and two saddle points remain.

Three saddle-node bifurcations: $\boldsymbol{\alpha_{min} < \alpha < \bar{\alpha}_{max}}$. Consider (21) with $\alpha_{min} < \alpha < \bar{\alpha}_{max}$. Since the qualitative behavior of the solutions of (21) with $\alpha_{min} < \alpha < \alpha_{max}$ are all similar, we show the results in an example with $\alpha = 1/3$.

As is clear from (21) and illustrated in Figure 8 (first row), choosing the heterogeneity of (20) maintains the $\dot{\theta}_2 = 0$ nullclines and only perturbs the $\dot{\theta}_1 = 0$ nullclines. This perturbation causes the topology of the $\dot{\theta}_1 = 0$ nullclines to change, combining the isolated loop with a nullcline that encircles the torus and thereafter reducing the number of fixed points.

In Figure 8 (first row), we show the nullclines of (21) with $\alpha = 1/3$ and increase δI_b from 0 to 0.015, where the first saddle-node bifurcation (shown by SN1) occurs and the unstable tripod gait (shown by N1) disappears, colliding with a saddle point (shown by S1). We further increase δI_b to 0.04 where the second saddle-node bifurcation (shown by SN2) occurs and the stable $\approx (2/3, 2/3)$ fixed point (shown by N2) disappears, colliding with a saddle point (shown by S2). Finally, when δI_b reaches 0.056, the third saddle-node bifurcation (shown by SN3) occurs and the stable forward tetrapod gait (shown by N3) disappears, colliding with a saddle point (shown by S3), and only one stable fixed point remains, which corresponds to the approximate backward tetrapod gait $\approx (0.25, 0.7)$, as we desired.

Two saddle-node bifurcations: $\boldsymbol{\alpha > \bar{\alpha}_{max}}$. We now consider (21) with $\alpha > \bar{\alpha}_{max}$. Since the qualitative behavior of the solutions of (21) with $\alpha > \bar{\alpha}_{max}$ are all similar, we only show the results for $\alpha \approx 0.95$. As illustrated in Figure 8 (second row), choosing the heterogeneity of (20) maintains the $\dot{\theta}_2 = 0$ nullclines and, by combining two $\dot{\theta}_1 = 0$ nullclines that encircle the torus, changes the topology of the $\dot{\theta}_1 = 0$ nullclines and thereafter, through two saddle-node bifurcations, reduces the number of fixed points. As δI_b increases from 0 to 0.0121, one saddle-node bifurcation (shown by SN1) occurs in which the unstable tripod gait (shown by N1) and the backward tetrapod gait (shown by S1) disappear; as δI_b increases further to 0.013, another saddle-node bifurcation (shown by SN2) occurs and the stable fixed point shown by N2 disappears and a unique stable approximate backward tetrapod gait remains at $(0.31, 0.69)$. The nullclines at $\delta I_b \approx 0.012$ are shown to illustrate how the $\dot{\theta}_1 = 0$ nullclines move toward each other and cause the saddle-node bifurcations.

Remark 1. In Table 1, we summarize the main results shown in Figures 5–8.
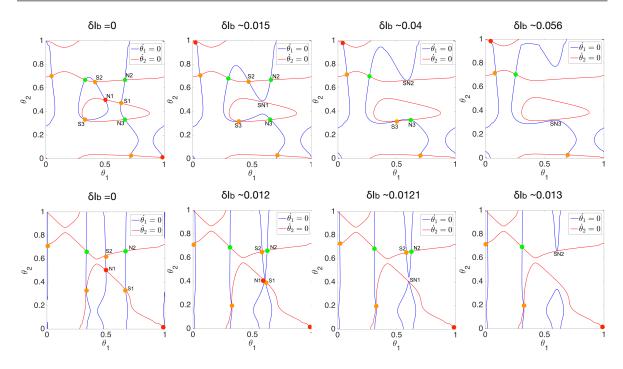
Figure 8. *Nullclines of* (21) *with* $I_{ext} = 35.65$ *are shown for* $\alpha = 1/3$ *(first row) and* $\alpha \approx 0.95$ *(second row) as the heterogeneity parameter* δI_b *varies. As discussed in section* 4.2, (21) *with* $\delta I_b = 0$ *possess either* 10 *(first row, left) or eight (second row, left) fixed points including a stable backward tetrapod gait. As* δI_b *increases, through three (first row) or two (second row) saddle-node bifurcations (shown by SN), six (first row) or four (second row) fixed points disappear and a single stable approximate backward tetrapod gait remains together with a source and two saddle points. Note that in the second row the second to left figure is topologically equivalent to the left figure and is included to show how the nullclines move. Nullclines and fixed points are colored as indicated in Figure* 4.

Table 1
A summary of Figures 5–8.

Figure	α	I_{ext}^1	I_{ext}^2	I_{ext}^3	Bifurcation type
5	Varies	0	0	0	1 transcritical & 1 saddle-node
6 (row 1)	$\bar{\alpha}_{min} < \alpha < \alpha_{max}$	$(= \delta I_f)$ varies	$(= \delta I_f)$ varies	0	3 saddle-nodes
6 (row 2)	$0 < \alpha < \bar{\alpha}_{min}$	$(= \delta I_f)$ varies	$(= \delta I_f)$ varies	0	2 saddle-nodes
7	varies	0	0	0	1 transcritical & 1 saddle-node
8 (row 1)	$\alpha_{min} < \alpha < \bar{\alpha}_{max}$	0	$(= \delta I_b)$ varies	$(= \delta I_b)$ varies	3 saddle-nodes
8 (row 2)	$\bar{\alpha}_{max} < \alpha$	0	$(= \delta I_b)$ varies	$(= \delta I_b)$ varies	2 saddle-nodes

4.3. Transition from the approximate tetrapod to the approximate tripod gait. In [1] we studied gait transitions from multiple tetrapod gaits (e.g., Figure 4 (left)) to a unique stable tripod gait as speed increases. In the current paper, we introduce approximate transition gaits $(1/3 + \eta, 2/3 - \eta)$ (resp., $(2/3 - \eta, 1/3 + \eta)$) and show that, for suitable heterogeneities, as η changes from 0 to $1/6$, they connect a single stable approximate forward (resp., backward) tetrapod gait to a single stable approximate tripod gait.

As an illustration, we show the gait transition in (14) when the c_i's satisfy (15), $\delta I \approx 0.038$, and I_{ext} increases from 35.65 to 37.5. In Figure 9, we observe that as I_{ext} increases, the unique
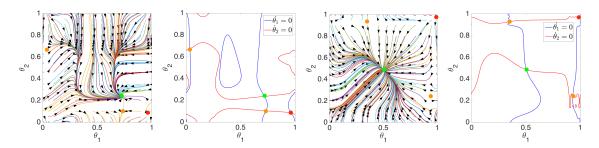
Figure 9. *(Left to right) Phase planes and nullclines of Equations* (14) *when c_i's satisfy Equation* (15), *$\delta I \approx 0.038$, and $I_{ext} = 35.65$ (the nullclines of which are also shown in Figure* 4 *(right panel)), and $I_{ext} = 37.5$, respectively. Nullclines and fixed points are colored as indicated in Figure* 4.

stable approximate forward tetrapod gait becomes a stable approximate tripod gait. The second and fourth figures show the nullclines and hence the positions of the fixed points for $I_{ext} = 35.65, 37.5$, respectively, and the first and third figures show the corresponding phase planes.

Note that the topology of the nullclines in Figure 9 is different. However, no bifurcation of fixed points occurs and the forward tetrapod gait continuously moves to the tripod gait, as speed increases.

5. Equivalent perturbations. In this section, we will show that perturbing the intrinsic dynamics of each unit of the CPG can be equivalent to perturbing the coupling function g or the coupling strengths c_i.

Recalling (29), we show that, under an appropriate condition on the c_i's, derived below, adding I_{ext}^i to each neuron i is equivalent to adding dI_j to the coupling function $g(x_i, x_j)$ that connects neuron i to its neighbor j, where dI_j is the unique solution of

$$
(22) \qquad
\begin{pmatrix} I_{ext}^1 \\ \vdots \\ I_{ext}^6 \end{pmatrix}
= \mathcal{C}
\begin{pmatrix} dI_1 \\ dI_2 \\ dI_3 \\ dI_4 \\ dI_5 \\ dI_6 \end{pmatrix}
:=
\begin{pmatrix}
0 & c_5 & 0 & c_1 & 0 & 0 \\
c_4 & 0 & c_7 & 0 & c_2 & 0 \\
0 & c_6 & 0 & 0 & 0 & c_3 \\
c_1 & 0 & 0 & 0 & c_5 & 0 \\
0 & c_2 & 0 & c_4 & 0 & c_7 \\
0 & 0 & c_3 & 0 & c_6 & 0
\end{pmatrix}
\begin{pmatrix} dI_1 \\ dI_2 \\ dI_3 \\ dI_4 \\ dI_5 \\ dI_6 \end{pmatrix}.
$$

For example, if the above equation has a unique solution, then since $I_{ext}^1 = c_5 dI_2 + c_1 dI_4$, adding I_{ext}^1 to unit 1 is equivalent to adding dI_2 to $g(x_1, x_2)$ and dI_4 to $g(x_1, x_4)$, i.e.,

$$
\begin{aligned}
\dot{x}_1 &= f(x_1) + I_{ext}^1 + c_1 g(x_1, x_4) + c_5 g(x_1, x_2) \\
&= f(x_1) + c_5 dI_2 + c_1 dI_4 + c_1 g(x_1, x_4) + c_5 g(x_1, x_2) \\
&= f(x_1) + c_1 (g(x_1, x_4) + dI_4) + c_5 (g(x_1, x_2) + dI_2).
\end{aligned}
$$

Equation (22) has a unique solution if the matrix $\mathcal{C}$ is nonsingular, i.e., $\det \mathcal{C} \neq 0$. The matrix $\mathcal{C}$ can be written as

$$
\mathcal{C} = \begin{pmatrix} \mathcal{A} & \mathcal{B} \\ \mathcal{B} & \mathcal{A} \end{pmatrix},
$$

where $\mathcal{A} = \begin{pmatrix} 0 & c_5 & 0 \\ c_4 & 0 & c_7 \\ 0 & c_6 & 0 \end{pmatrix}$ and $\mathcal{B} = \operatorname{diag}(c_1, c_2, c_3)$. Since

$$\begin{pmatrix} I & 0 \\ I & I \end{pmatrix} \begin{pmatrix} \mathcal{A} & \mathcal{B} \\ \mathcal{B} & \mathcal{A} \end{pmatrix} \begin{pmatrix} I & 0 \\ -I & I \end{pmatrix} = \begin{pmatrix} \mathcal{A} - \mathcal{B} & \mathcal{B} \\ 0 & \mathcal{A} + \mathcal{B} \end{pmatrix},$$

where I and 0 are identity and zero matrices of appropriate sizes, and as shown in [13],

$$\det \begin{pmatrix} \mathcal{A} - \mathcal{B} & \mathcal{B} \\ 0 & \mathcal{A} + \mathcal{B} \end{pmatrix} = \det(\mathcal{A} - \mathcal{B}) \det(\mathcal{A} + \mathcal{B}),$$

we have

$$\det \mathcal{C} = \det(\mathcal{A} - \mathcal{B}) \det(\mathcal{A} + \mathcal{B}) = \det \begin{pmatrix} -c_1 & c_5 & 0 \\ c_4 & -c_2 & c_7 \\ 0 & c_6 & -c_3 \end{pmatrix} \det \begin{pmatrix} c_1 & c_5 & 0 \\ c_4 & c_2 & c_7 \\ 0 & c_6 & c_3 \end{pmatrix}$$
$$= -(c_1 c_2 c_3 - c_1 c_6 c_7 - c_3 c_4 c_5)^2.$$

Hence, $\mathcal{C}$ is nonsingular if and only if $c_1 c_2 c_3 - c_1 c_6 c_7 - c_3 c_4 c_5 \neq 0$.

Next, we show that perturbing each CPG unit by an external current can be equivalent to perturbing the coupling strengths. Recalling (7) and Assumptions 2 and 4, adding I_{ext}^i to each unit i is equivalent to adding $\Delta_i := \tilde{\omega}_i / H(2/3 - \eta; \xi)$ to the contralateral coupling c_i, $i = 1, 2, 3$, and keeping the other coupling strengths unchanged. Note that $\tilde{\omega}_i$ is of order ϵ and H is of order 1; therefore Δ_i is of order ϵ.

For example, adding I_{ext}^1 to unit 1 is equivalent to adding $\tilde{\omega}_1$ to the corresponding phase equation; therefore by Assumption 4, we get

$$\dot{\phi}_1 = \omega + \tilde{\omega}_1 + c_1 H(\phi_4 - \phi_1; \xi) + c_5 H(\phi_2 - \phi_1; \xi)$$
$$= \omega + \tilde{\omega}_1 + c_1 H(2/3 - \eta; \xi) + c_5 H(\phi_2 - \phi_1; \xi)$$
$$= \omega + \frac{\tilde{\omega}_1}{H(2/3 - \eta; \xi)} H(2/3 - \eta; \xi) + c_1 H(2/3 - \eta; \xi) + c_5 H(\phi_2 - \phi_1; \xi)$$
$$= \omega + \left(\frac{\tilde{\omega}_1}{H(2/3 - \eta; \xi)} + c_1 \right) H(2/3 - \eta; \xi) + c_5 H(\phi_2 - \phi_1; \xi)$$
$$= \omega + (\Delta_1 + c_1) H(2/3 - \eta; \xi) + c_5 H(\phi_2 - \phi_1; \xi).$$

6. Discussion. In [1] we studied a homogeneous interconnected phase oscillator model for insect locomotion, and we showed that the cyclic motion of each leg can be described by an oscillator and that the insect's speed increases with the common external input, I_{ext}, that each leg receives. At high speeds, when I_{ext} is large, the model generates a unique stable tripod gait, as observed experimentally in cockroaches and fruit flies. However, for small I_{ext}, the model's low speed dynamics include both stable forward and backward tetrapod gaits and a stable gait that has not been observed in insects, in which triple, double, and single swing phases occur [1, Figure 29]. While fruit flies exhibit forward and backward tetrapod

gaits at low speeds, the latter have only been seen in backward walking [12], and we therefore propose that brain or central nervous system inputs are likely used to switch among and select particular gaits.

In the present paper, we relax the assumption of homogeneous oscillators and allow heterogeneous ipsilateral external inputs denoted by $I_{ext} + I_{ext}^i(t)$ for $i = 1, 2, 3$. Preserving contralateral symmetry of inputs, we find that, at low speed with small I_{ext}, and appropriate choices of small heterogeneities $I_{ext}^i(t)$, $i = 1, 2, 3$, the heterogeneous model generates only one stable approximate forward or backward tetrapod gait, as is observed experimentally. The selection of a stable gait is accomplished via sequences of saddle-node bifurcations in which all but one of the stable gaits disappears as particular currents $I_{ext}^i(t)$ increase. See Table 1 for a summary of the behaviors presented in section 4.

The paper [4], noted in our introduction, achieves similar effects on interunit phase differences via short excitatory and inhibitory "global stimuli" which move the network's state into the domain of attraction of a desired stable fixed point, while multiple stable fixed points continue to coexist. In contrast, our heterogeneous inputs eliminate stable states via bifurcations, thereby shepherding the system's state toward a new stable fixed point.

At high speeds the single stable solution of the heterogeneous model is a tripod gait, as in the homogeneous case, and the model exhibits a transition from a forward or a backward tetrapod to a tripod gait as I_{ext} increases (see Figure 9 for the former case).

In future work, we propose to allow the heterogeneous external inputs to be *noisy* and to study the resulting effects on the existence of gaits and their transitions.

Appendix. A network of weakly interconnected bursting neurons. In [1, section 2.1], we employed an ion-channel bursting neuron model for an insect CPG which was developed in [9, 14]. The bursting neuron model of each unit of the CPG contains a system of four ODEs describing transmembrane cell voltages, slow and fast ionic gates, and the dynamics of neurotransmitter release at synapses, as follows:

$$C\dot{v} = -\{I_{Ca}(v) + I_K(v, m) + I_{KS}(v, w) + I_L(v)\} + I_{ext}, \tag{23a}$$

$$\dot{m} = \frac{\gamma}{\tau_m(v)}[m_\infty(v) - m], \tag{23b}$$

$$\dot{w} = \frac{\delta}{\tau_w(v)}[w_\infty(v) - w], \tag{23c}$$

$$\dot{s} = \frac{1}{\tau_s}[s_\infty(v)(1 - s) - s], \tag{23d}$$

where the ionic currents are of the following forms:

$$
\begin{aligned}
I_{Ca}(v) &= \bar{g}_{Ca} n_\infty(v)(v - E_{Ca}), & I_K(v, m) &= \bar{g}_K\, m\, (v - E_K), \\
I_{KS}(v, w) &= \bar{g}_{KS} w\, (v - E_{KS}), & I_L(v) &= \bar{g}_L(v - E_L).
\end{aligned}
\tag{24}
$$

The steady state gating variables associated with ion channels and their time scales take the forms

$$
\begin{aligned}
m_\infty(v) &= \frac{1}{1 + e^{-2k_K(v - v_K)}}, & w_\infty(v) &= \frac{1}{1 + e^{-2k_{KS}(v - v_{KS})}}, \\
n_\infty(v) &= \frac{1}{1 + e^{-2k_{Ca}(v - v_{Ca})}}, & s_\infty(v) &= \frac{a}{1 + e^{-2k_s(v - E_s^{pre})}},
\end{aligned}
\tag{25}
$$

Table 2
The constant parameters in the bursting neuron model.

I_{ext}	$\bar{g}_{Ca}$	$\bar{g}_K$	$\bar{g}_{KS}$	$\bar{g}_L$	$\bar{g}_{syn}$	E_{Ca}	E_K	E_{KS}	E_L	E_s^{post}	E_s^{pre}
Varies	4.4	9.0	0.5	2.0	0.01	120	-80	-80	-60	-70	2

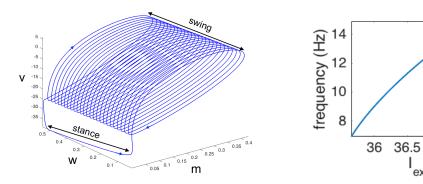| k_{Ca}	k_K	k_{KS}	k_s	v_{Ca}	v_K	v_{KS}	a	C	γ	τ_s	δ
0.056	0.1	0.8	0.11	-1.2	2	-26	444.48	1.2	5.0	5.56	0.027

Figure 10. *Left: A periodic orbit of the bursting neuron model, equation* (23), *in* (v, m, w) *space. Right: The effect of I_{ext} on the stepping frequency of the periodic orbit.*

and

$$(26) \qquad \tau_m(v) = \text{sech}\left(0.5\, k_K(v - v_K)\right), \quad \tau_w(v) = \text{sech}\left(0.5\, k_K(v - v_{KS})\right).$$

The external current I_{ext}, which represents input from the central nervous system and brain, varies between 35.65 and 37.7 as speed increases. Other parameters are generally fixed as specified in Table 2 and are chosen such that the model (23) possesses an attracting hyperbolic limit cycle Γ. Most of the parameter values are taken from [14], but some of our notation is different. See [1, section 2.1] for further details of the model and its parameters.

As shown in Figure 10 (left), the periodic orbit in (v, m, w) space contains a sequence of spikes (a burst) followed by a quiescent phase, which correspond respectively to the swing and stance durations of one leg. The burst from the CPG inhibits depressor motoneurons and excites levator motoneurons, allowing the swing leg to lift from the ground [9, Figure 2] and [15, Figure 11] (see also [16, 17]). We denote the period of the periodic orbit by T, i.e., it takes T time units (ms here) to complete the stance and swing cycle of each leg. The number of steps completed by one leg per unit of time is the stepping frequency and is equal to $\omega = 2\pi/T$. In [1, Figure 2], we observed that as one of the two parameters in the bursting neuron model, either the slow time scale δ or the external current I_{ext}, increases, the period of the periodic orbit decreases, primarily by decreasing stance duration, and so the insect's speed increases. There, we used these parameters as speed parameters, denoted by ξ, and studied transitions from tetrapod to tripod gaits as ξ increases. To see how I_{ext} affects the frequency of the periodic orbit, see Figure 10 (right).

In [1], we assumed that inhibitory coupling is achieved via synapses that produce negative postsynaptic currents. The synapse variable s enters the postsynaptic cell in (23a) as an additional term, I_{syn},

$$(27) \qquad C\dot{v}_i = -\{I_{Ca} + I_K + I_{KS} + I_L\} + I_{ext} + I_{syn},$$

where

$$(28) \qquad I_{syn} = \sum_{j \in \mathcal{N}_i} I_{syn}(v_i, s_j) = \sum_{j \in \mathcal{N}_i} -\bar{c}_{ji}\bar{g}_{syn}s_j\left(v_i - E_s^{post}\right),$$

$\bar{g}_{syn}$ denotes the synaptic strength, and $\mathcal{N}_i$ denotes the set of the nodes adjacent to node i. The multiplicative factor $\bar{c}_{ji}$ accounts for the fact that multiple bursting neurons are interconnected in the insects, and $-\bar{c}_{ji}\bar{g}_{syn}$ represents an overall coupling strength between hemisegments. Following [8] we assumed contralateral symmetry and included only nearest neighbor coupling, so that there are three contralateral coupling strengths c_1, c_2, c_3 and four ipsilateral coupling strengths c_4, c_5, c_6, and c_7; see Figure 1. For example, $\bar{c}_{21} = c_5$, $\bar{c}_{41} = c_1$, etc. We chose reversal potentials E_s^{post} that make all synaptic connections inhibitory; this implies that the c_i's are positive.

The following system of 24 ODEs describes the dynamics of the six coupled cells in the network as shown in Figure 1. We assume that each cell, which is governed by (23), represents one leg of the insect. Cells $1, 2$, and 3 represent right front, middle, and hind legs, and cells $4, 5$, and 6 represent left front, middle, and hind legs, respectively:

$$(29) \qquad \begin{aligned} \dot{x}_1 &= f(x_1) + c_1 g(x_1, x_4) + c_5 g(x_1, x_2), \\ \dot{x}_2 &= f(x_2) + c_2 g(x_2, x_5) + c_4 g(x_2, x_1) + c_7 g(x_2, x_3), \\ \dot{x}_3 &= f(x_3) + c_3 g(x_3, x_6) + c_6 g(x_3, x_2), \\ \dot{x}_4 &= f(x_4) + c_1 g(x_4, x_1) + c_5 g(x_4, x_5), \\ \dot{x}_5 &= f(x_5) + c_2 g(x_5, x_2) + c_4 g(x_5, x_4) + c_7 g(x_5, x_6), \\ \dot{x}_6 &= f(x_6) + c_3 g(x_6, x_3) + c_6 g(x_6, x_5), \end{aligned}$$

where $x_i = (v_i, m_i, w_i, s_i)^\top$, $f(x_i)$ is as the right-hand side of (23), and

$$(30) \qquad g(x_i, x_j) = \left(-\bar{g}_{syn}s_j\left(v_i - E_s^{post}\right), 0, 0, 0\right)^\top$$

is the coupling function with a small synaptic coupling strength $\bar{g}_{syn}$. This assumption of weak coupling is necessary for the use of phase reduction in section 2.

This 6-bursting neuron model was used to drive agonist-antagonist muscle pairs in a neuromechanical model with jointed legs that reproduced the dynamics of freely running cockroaches [18]; also see [19]. These papers and subsequent phase-reduced models [20, 8] support our belief that the bursting neuron model is capable of producing realistic inputs to muscles in insects. In [1, Figures 5 and 6], we showed that the 24 ODEs coupled bursting neuron model with small I_{ext} (or δ) can produce a tetrapod gait with two legs lifted off the ground simultaneously in swing, and as I_{ext} (or δ) increases, it can produce a tripod gait with three legs lifted off the ground simultaneously in swing.

REFERENCES

[1] Z. AMINZARE, V. SRIVASTAVA, AND P. HOLMES, *Gait transitions in a phase oscillator model of an insect central pattern generator*, SIAM J. Appl. Dyn. Syst., 17 (2018), pp. 626–671.

[2] J. WOJCIK, J. SCHWABEDAL, R. CLEWLEY, AND A. L. SILNIKOV, *Key bifurcations of bursting polyrhythms in 3-cell central pattern generators*, PLoS ONE, 9 (2014), e92918.

[3] R. BARRIO, M. RODRÍGUEZ, S. SERRANO, AND A. SILNIKOV, *Mechanism of quasi-periodic lag jitter in bursting rhythms by a neuronal network*, European Phys. Lett., 112 (2015), 38002.

[4] A. LOZANO, M. RODRÍGUEZ, AND R. BARRIO, *Control strategies of 3-cell central pattern generator via global stimuli*, Scientific Reports, 6 (2016), 23622.

[5] M. AGUIAR, P. ASHWIN, A. DIAS, AND M. FIELD, *Dynamics of coupled cell networks: Synchrony, heteroclinic cycles and inflation*, J. Nonlinear Sci., 21 (2011), pp. 271–323.

[6] M. A. SCHWEMMER AND T. J. LEWIS, *The theory of weakly coupled oscillators*, in Phase Response Curves in Neuroscience: Theory, Experiment, and Analysis, N. W. Schultheiss, A. A. Prinz, and R. J. Butera, eds., Springer, New York, 2012.

[7] Y. KURAMOTO, *Chemical Oscillations, Waves, and Turbulence*, Springer Ser. Synergetics, 19, Springer-Verlag, Berlin, 1984.

[8] E. COUZIN-FUCHS, T. KIEMEL, O. GAL, A. AYALI, AND P. HOLMES, *Intersegmental coupling and recovery from perturbations in freely running cockroaches*, J. Exp. Biol., 218 (2015), pp. 285–297.

[9] R. M. GHIGLIAZZA AND P. HOLMES, *A minimal model of a central pattern generator and motoneurons for insect locomotion*, SIAM J. Appl. Dyn. Syst., 3 (2004) pp. 671–700.

[10] C. RADHAKRISHNA RAO AND S. KUMAR MITRA, *Generalized Inverse of Matrices and its Applications*, John Wiley & Sons, New York, 1971.

[11] A. YELDESBAY, T. TÓTH, AND S. DAUN, *The role of phase shifts of sensory inputs in walking revealed by means of phase reduction*, J. Comput. Neurosci., 44 (2018), pp. 313–339.

[12] S. S. BIDAYE, C.MACHACEK, Y. WU, AND B. J. DICKSON, *Neuronal control of drosophila walking direction*, Science, 344 (2014), pp. 97–101.

[13] J. R. SILVESTER, *Determinants of block matrices*, Math. Gazette, 84 (2000), pp. 460–467.

[14] R. M. GHIGLIAZZA AND P. HOLMES, *Minimal models of bursting neurons: The effects of multiple currents and timescales*, SIAM J. Appl. Dyn. Syst., 3 (2004), pp. 636–670.

[15] K. G. PEARSON AND J. F. ILES *Nervous mechanisms underlying intersegmental co-ordination of leg movements during walking in the cockroach*, J. Exp. Biol., 58 (1973), pp. 725–744.

[16] K. G. PEARSON AND J. F. ILES, *Discharge patterns of coxal levator and depressor motoneurons of the cockroach*, Periplaneta americana, J. Exp. Biol., 52 (1970) pp. 139–165.

[17] K. G. PEARSON, *Central programming and reflex control of walking in the cockroach*, J. Exp. Biol., 56 (1972), pp. 173–193.

[18] R. P. KUKILLAYA, J. L. PROCTOR, AND P. HOLMES, *Neuromechanical models for insect locomotion: Stability, maneuverability, and proprioceptive feedback*, Chaos, 19 (2009) 026107.

[19] R. P. KUKILLAYA AND P. HOLMES, *A model for insect locomotion in the horizontal plane: Feedforward activation of fast muscles, stability, and robustness*, J. Theoret. Biol., 261 (2009), pp. 210–226.

[20] J. PROCTOR, R. P. KUKILLAYA, AND P. HOLMES, *A phase-reduced neuro-mechanical model for insect locomotion: Feed-forward stability and proprioceptive feedback*, Philos. Trans. Roy. Soc. A, 368 (2010), pp. 5087–5104.